Journal of Glaciology

Article

Cite this article: Ohno H, Iizuka Y, Fujita S (2021). Pure rotational Raman spectroscopy applied to N_2/O_2 analysis of air bubbles in polar firn. *Journal of Glaciology* **67**(265), 903–908. https://doi.org/10.1017/jog.2021.40

Received: 28 January 2021
Revised: 25 March 2021
Accepted: 25 March 2021
First published online: 26 April 2021

Key words:
Antarctic glaciology; ice core; polar firn

Author for correspondence:
Hiroshi Ohno,
E-mail: h_ohno@mail.kitami-it.ac.jp

cambridge.org/jog

Pure rotational Raman spectroscopy applied to N_2/O_2 analysis of air bubbles in polar firn

Hiroshi Ohno[1], Yoshinori Iizuka[2] and Shuji Fujita[3,4]

[1]Kitami Institute of Technology, Kitami, Japan; [2]Institute of Low Temperature Science, Hokkaido University, Sapporo, Japan; [3]National Institute of Polar Research, Research Organization of Information and Systems (ROIS), Tokyo, Japan and [4]Department of Polar Science, School of Multidisciplinary Sciences, The Graduate University for Advanced Studies, SOKENDAI, Miura, Japan

Abstract

Earlier gas measurements of firn air (atmosphere in open pore channels) at polar sites have revealed the occurrence of gas fractionation phenomena during bubble close-off, in addition to well-known thermal and gravitational gas separation. Nevertheless, because of difficulties posed by measurement, little is known about the distribution of air constituents in already closed pores (bubbles) in firn. Herein, we describe the application of high-sensitivity pure rotational Raman spectroscopy, combined with sample immersion in the fluorocarbon-based inert fluid for removing the optical disturbance by diffused reflection. That application efficiently elicits information about nitrogen and oxygen composition ratios (N_2/O_2 or O_2/N_2) for each air bubble in firn. The developed methodology presents important implications for elucidating how gas records are formed and modified in the course of pore close-off in polar firn.

1. Introduction

When polar firn transforms into ice, i.e. loss of permeability, the surrounding atmospheric gases are trapped in the ice matrix as air bubbles (e.g. Cuffey and Paterson, 2010). In the depths of inland ice sheets, air bubbles crystallize into air clathrate hydrates (Shoji and Langway, 1982). The air constituents preserved in the air bubbles and hydrates (air inclusions) provide unique archives to reconstruct past atmospheric compositions (e.g. Petit and others, 1999). Moreover, gases extracted from polar ice cores are useful as various climate proxies. For example, the composition ratio of nitrogen and oxygen, N_2/O_2 (or O_2/N_2), is known to co-vary with local summer insolation (Bender, 2002). Such ratios are therefore used to construct an ice core chronology (Kawamura and others, 2007). Although little is known about how the N_2/O_2 climate signal forms, it is believed to originate from changes in surface-snow texture caused by solar radiation: the snow texture might determine the duration of firn-to-ice transition and thus might determine the degree of gas fractionation during bubble close-off (Fujita and others, 2009; Lipenkov and others, 2011).

For correct interpretation of gas records, understanding of processes in ice sheets that alter gas compositions is crucially important. In the most upper part of firn, bulk movement of gases (convection) can mix air rapidly inside pores with the atmosphere above the snow surface. However, at deeper depths, where air is stagnant, the dominant mechanism for gas transport is molecular diffusion. In deep firn, heavier gas components tend to settle to the bottom of firn because of gravity effects (Craig and others, 1988), while they are also subject to migration towards colder regions (Severinghaus and others, 2001), both resulting in gas fractionation. Moreover, in the process of bubble close-off, gas separation is regarded as occurring during gas transport from compressed air bubbles to open pores connected to the atmosphere because of differences in diffusivity through the lattice of ice crystals between gas species (Huber and others, 2006; Severinghaus and Battle, 2006). Even in deep ice, the modification of gas compositions is unavoidable: molecular-size-dependent gas diffusion from air bubbles to hydrates is known to take place at depths where air bubbles and clathrate hydrates coexist (the so-called bubble-to-hydrate transition zone) (Ikeda and others, 1999; Ikeda-Fukazawa and others, 2001).

Micro-Raman spectroscopy, which can provide information about the gas composition of each air inclusion (Nakahara and others, 1987), is a powerful tool to investigate gas fractionation phenomena in polar ice, as described below. Measurements of N_2/O_2 inside individual air bubbles at various depths in the EDML Antarctic ice core were performed by Weikusat and others (2012). They found that small bubbles, with a diameter less than 200 μm, in deep ice are enriched markedly in O_2 compared to larger bubbles. They inferred that phenomenon to be an effect of pressure relaxation during storage of the core. Considerable gas fractionation has been found from micro-Raman analyses of air inclusions in the bubble-to-hydrate transition zones of Vostok and Dome Fuji, Antarctica (Ikeda and others, 1999; Ikeda-Fukazawa and others, 2001). These observations show clearly that O_2 is enriched in clathrate hydrates, while it is depleted in air bubbles. The observed differences in N_2/O_2 between the air bubbles and hydrates in the transition zones have been attributed to higher gas permeation (the product of gas diffusivity and solubility) of O_2 in the ice matrix than that of N_2.

Only one report in the relevant literature describes the application of micro-Raman spectroscopy to the investigation of air bubbles in firn (Ikeda and others, 1999), probably because of two difficulties related to measurement. The first difficulty is detection of the extremely weak Raman signals from firn samples. Because of the low overburden pressure, the density of gases inside bubbles is lower in firn than in deep ice, considerably reducing the Raman scattering intensity. The second difficulty is microscopic observation inside 'un-transparent' firn. In firn, snow–air interfaces with large areas and irregular shapes give rise to the strongly-diffused reflection of the observation light that severely disturbs the optical path for measurement. Consequently, earlier work necessarily relied on extremely long laser exposure times (a few hours) to obtain a single spectrum from a shallow sample (Ikeda and others, 1999). In this work, we demonstrate that the combined use of pure rotational Raman spectroscopy and the inert-fluid immersion method can overcome these difficulties.

2. Methods

Instead of using traditional vibrational Raman spectroscopy, we have applied pure rotational Raman spectroscopy to the measurement of air bubbles in polar firn.

Pure rotational energy levels of a linear molecule such as N_2 or O_2 in the rotational quantum state J are

$$E_J = [BJ(J+1) - DJ^2(J+1)^2]hc, \quad J = 0,\ 1,\ 2,\ \ldots \qquad (1)$$

where h is Planck's constant, c represents the velocity of light, B is the rotational constant and D is the centrifugal distortion constant (Atkins and Paula, 2014). Because of the rotational Raman selection rule, the energy-level transitions with $\Delta J = \pm 2$ (change in the rotational quantum number is $+2$ or -2) are Raman-active for a linear molecule (Atkins and Paula, 2014). $\Delta J = +2$ corresponds to Stokes Raman scattering, while $\Delta J = -2$ corresponds to antiStokes Raman scattering. Because of strong scattering intensity, Stokes scattering rather than antiStokes scattering is usually analyzed in Raman spectroscopy.

The differential backscatter cross section for a Stokes line of the pure rotational Raman spectrum is

$$\sigma = \frac{112\pi^4}{15}\frac{ghcB(\nu_0+\Delta\nu)^4\gamma^2}{(2I+1)^2kT}\frac{(J+1)(J+2)}{(2J+3)}exp\left(-\frac{E_J}{kT}\right), \quad J = 0,\ 1,\ 2,\ \ldots \qquad (2)$$

where g is the statistical weight factor, which depends on the nuclear spin I. Also, ν_0 stands for the incident light frequency, $\Delta\nu$ denotes the frequency shift, γ signifies the anisotropy of the molecular polarizability tensor, k is Boltzman's constant and T expresses the temperature (Penny and others, 1974). The intensity in a pure rotational line is proportional to σ, the incident light power and the density of molecules of interest.

In the pure rotational Raman spectra, as a result of nuclear statistics, N_2 shows alternation in intensity (Fig. 1), whereas transitions between even values of J are missing in O_2 (Fig. 1). A pure rotational Raman spectrum of air is regarded as the superposition of the Raman lines from N_2 and O_2 (Fig. 2). Pure rotational Raman signals from other Raman-active species in air, such as CO_2, are too small compared with those of the two dominant atmospheric components. As depicted in Figure 3, Raman scattering of air (N_2 and O_2) from pure rotational modes is considerably stronger than that from vibrational modes, providing a benefit for the measurement of N_2 and O_2 gases with low density, as in the case for air bubbles in polar firn. Deconvolving heavily overlapped lines from N_2 and O_2 into two peaks is difficult (Fig. 2). Measurements of minor lines usually result in a poor signal-to-noise ratio, giving rise to considerable experimental error. Therefore, for this study, N_2/O_2 in air bubbles in polar firn was estimated by analyzing the pure rotational Raman intensities of strong and isolated lines.

$$\frac{N_2}{O_2} = \alpha\frac{I_{N_2,J4\to6} + I_{N_2,J5\to7} + I_{N_2,J7\to9} + I_{N_2,J8\to10} + I_{N_2,J10\to12} + I_{N_2,J11\to13}}{I_{O_2,J7\to9} + I_{O_2,J11\to13} + I_{O_2,J15\to17}} \qquad (3)$$

In that equation, α is a correction factor (an apparatus-dependent constant), I_{N_2} and I_{O_2}, respectively represent the scattering intensities of pure rotational Raman lines for N_2 and O_2, and subscript $J_{x\to x+2}$ denotes the energy-level transition which causes pure rotational Raman scattering (Figs 1, 2). By analyzing the relative intensities of pure rotational Raman lines in ambient atmospheric air ($N_2/O_2 = 3.7$), α in our experimental setup was found to be 2.0.

We used Fluorinert FC-40^{TM} (3M Inc.), a stable fluorocarbon-based transparent fluid, to suppress diffused reflection at snow–air interfaces. The pour point and density of FC-40 are, respectively, −57°C and 1.87 g cm^{-3} at 25°C. Importantly, its water solubility is extremely low (<5 ppmw). Also, its refractive index (1.29 at 25°C) is very close to that of ice (1.31). By replacing atmospheric gas with the Fluorinert, the intensity of diffused reflection at the interfaces is reduced by two orders of magnitude. As portrayed in Figure 4, 'white' firn becomes 'transparent' with the Fluorinert-immersion technique, thereby enabling microscopic observation inside firn. A Raman spectrum of Fluorinert FC-40 exhibits no lines in the low-frequency range (<120 cm^{-1}). It, therefore, does not disturb the pure rotational Raman measurement of air.

An Antarctic firn core (JARE39) was analyzed to test the new methods described above. The JARE39 core, 108 m long, was retrieved by the 39th Japanese Antarctic Research Expedition (JARE39) in 1998 at the Dome Fuji station (77°19′S 39°42′E). This site is characterized by annual mean temperature of −54°C and annual accumulation rate of 25.2 (±0.2) kg m^{-2} a^{-1} (Igarashi and others, 2011). After transportation to the Institute of Low Temperature Science, Hokkaido University, Sapporo, Japan, the firn core was stored in a cold room at −50°C. The pore close-off depth at Dome Fuji was estimated as ~104 m (Watanabe and others, 1997). In inland Antarctica, pore closure takes place mostly in the deepest several tens of meters of the firn (Burr and others, 2018). Consequently, firn cores at depths of 51 and 90 m (the former and latter, respectively correspond to the initial and middle stages of the closure process) were used as test samples. Densities at 51 and 90 m were estimated, respectively, as 655 and 795 kg m^{-3} (Fujita and others, 2016). Samples were prepared in a cold room at −20°C. Using a band saw, the innermost parts of the core 94 mm in diameter were cut into sections ~7 mm thick, 7 mm width and 30 mm long along the core axis (Fig. 4). The firn section was put into an optical cell made of quartz glass (10 × 10 × 58 mm) with a screw cap. Then the cell was filled with Fluorinert FC-40 precooled at −20°C (Fig. 4). The firn sample immersed in Fluorinert FC-40 was transferred to a cold chamber of a spectrometer set at −15°C.

Details of the cold chamber and sample-cooling system were presented in an earlier report by Sakurai and others (2010). In prior work, the temperature inside the chamber was controlled by regulating the flow rate of cold N_2 gas evaporated from liquid nitrogen, but the N_2 gas surrounding a sample gives rise to

https://doi.org/10.1017/jog.2021.40 Published online by Cambridge University Press

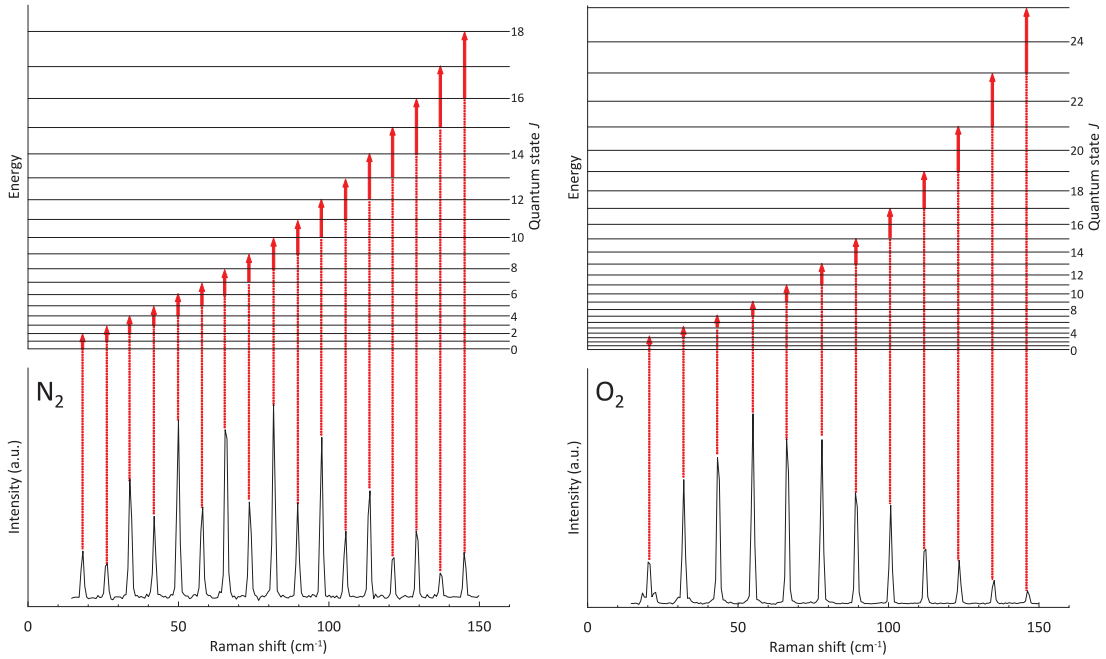

Fig. 1. Pure rotational Raman spectra of N_2 and O_2 measured at −15°C and 0.1 MPa. Schematics above the spectra indicate pure-rotational energy-level transitions which cause each Raman line.

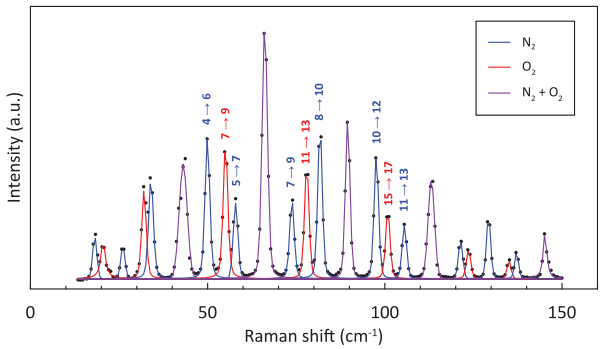

Fig. 2. Pure rotational Raman spectra of air at −15°C and 0.5 MPa. Numbers above lines denote the energy-level transition which causes the lines.

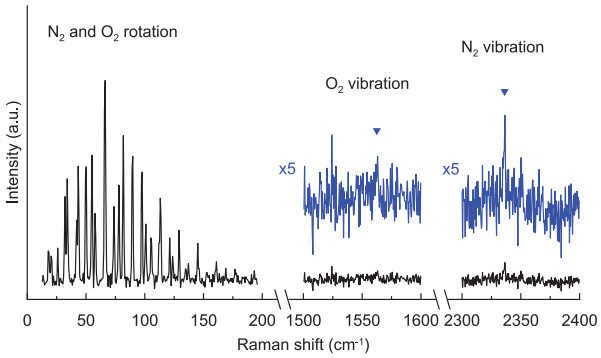

Fig. 3. Pure rotational and vibrational Raman spectra of ambient air at room temperature and atmospheric pressure.

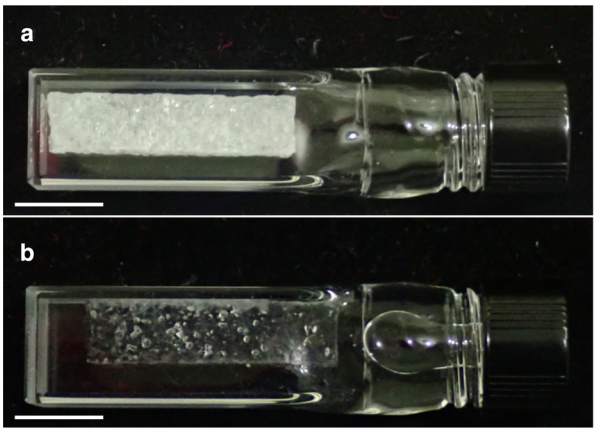

Fig. 4. Firn section of the JARE39 core (from 51 m depth) in the optical cell: (a) in air and (b) immersed in the fluorocarbon-based inert fluid (Fluorinert FC-40^{TM}). The scale bar in each image is 1 cm.

noticeable background Raman scattering in pure rotational Raman measurements because of large scattering cross-sections for the rotational modes. Consequently, in place of liquid nitrogen, liquid argon, which is Raman-inactive, was used as a coolant for this experiment. Pure rotational Raman spectra of samples were obtained using a triple monochromator (T6400; Horiba, Ltd.) with three 1800 gr. mm^{-1} gratings (Plane Holographic Package Aberration Correction Grating; Horiba, Ltd.), and a CCD detector (Symphony II; Horiba, Ltd.). The subtractive configuration of the monochromator was used for pure rotational Raman measurements: in the subtractive mode, the first and second gratings function as a filter to remove Rayleigh scattering, enabling one to obtain spectral information very close to the laser line (Gauglitz and Vo-Dinh, 2003). Incidentally, for a spectrometer with a single grating, which cannot use the subtractive mode, low-wavenumber Raman measurements can be achieved by installing an ultra-narrow-line notch filter in the spectrophotometer system (Glebov and others, 2012). Air bubbles inside the firn were observed using a microanalysis system (RSM-500; Horiba, Ltd.) connected to the monochromator. Laser light of 532 nm wavelength with the power of 700 mW (mpc3000; Laser Quantum) was focused on a bubble through the optical window of the cell using a long-working-distance objective lens with a focal length of 13 mm (M Plan Apo 50×; Mitutoyo Corp.). Backscattered light was corrected with the objective lens and

https://doi.org/10.1017/jog.2021.40 Published online by Cambridge University Press

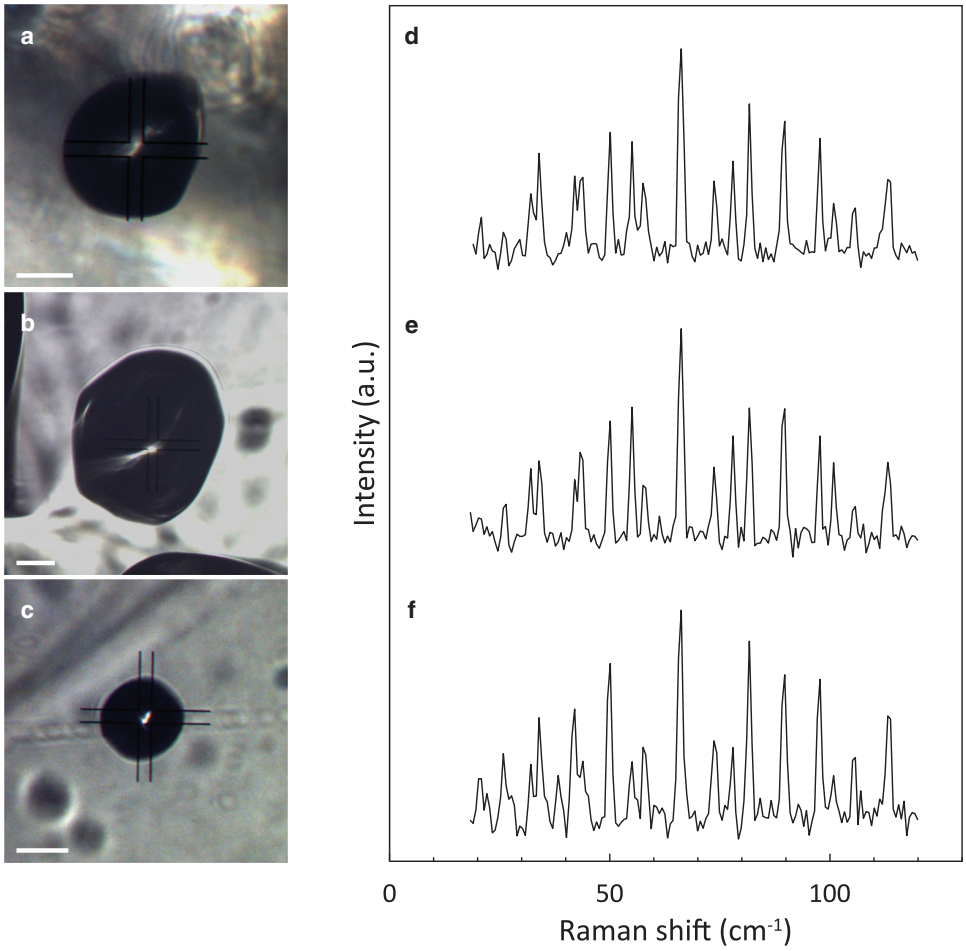

Fig. 5. (Left) Micrographs of air bubbles in the firn from depths of 51 m (a) and 90 m (b, c). The scale bar in each image is 50 μm. (Right) Pure rotational Raman spectra of the bubbles. Panels d–f, respectively, portray the spectra of bubbles (a–c).

Table 1. N_2/O_2 of air bubbles in the JARE39 firn core, where SE denotes a standard error of the N_2/O_2 measurements

Depth (m)	N_2/O_2	SE × 2
51	4.1	0.8
51	4.3	0.5
90	6.1	0.2
90	8.8	1.9
90	5.7	0.6
90	3.6	0.4
90	3.9	0.2
90	4.1	0.2

was sent to the spectrometer system. Using the multi-channel CCD detector, superimposed pure rotational Raman spectra from N_2 and O_2 were acquired at the same time (Fig. 2). It is noteworthy that distant vibrational Raman lines from N_2 and O_2 (Fig. 3) are usually recorded separately. The simultaneous signal acquisition for N_2 and O_2 provides better accuracy of the relative line intensity between the two components. This is because the optical path and laser focal point during measurement, which may change with time due to various factors (e.g. thermal drift of a sample) in the case of the separate signal acquisition, are regarded as being completely the same for the two components. The acquisition time for one spectrum was 180 s. Raman frequencies were calibrated using neon emission lines. To estimate N_2/O_2 using Eqn (3), deconvolution of the pure rotational Raman lines was performed using a commercial peak-fitting program (GRAMS/AI; Galactic Industries Corp.).

3. Results and discussion

Through the window of the optical cell and the Fluorinert, air bubbles inside the firn were clearly observable (Figs 5a–c). Figures 5d–f show that, despite the short data acquisition time, the simultaneous use of pure rotational Raman spectroscopy and the inert-fluid immersion technique can support sufficient intensity of Raman lines for analyses of air bubbles inside firn. For each air bubble, measurements were repeated 5–8 times. The mean N_2/O_2 values calculated using Eqn (3) are presented in Table 1. Additionally, twice the standard errors of N_2/O_2 calculations are shown as measurement errors (Table 1). The range of measurement errors was 0.2–1.9, depending on the scattering intensity from a bubble.

At 51 m, two air bubbles were analyzed (Table 1). The composition ratios of N_2 and O_2 for the bubbles are presented, respectively, as 4.1 and 4.3 (Table 1). Although these values are slightly larger than that of the atmospheric composition (3.7), the observed differences are within experimental error (twice the standard error). To clarify this point, further measurements are necessary.

At 90 m, six air bubbles were investigated (Table 1). It is particularly interesting that N_2/O_2 values in this sample were observed over the wide range of 3.6–8.8 (Table 1). Judging from the reproducibility of N_2/O_2 measurements (SE × 2 in Table 1), differences in the measurements between the bubbles are significant in most cases. For most bubbles, N_2/O_2 values are significantly higher than the atmospheric composition. Enrichment of nitrogen (depletion of oxygen) in bubbles was also reported

https://doi.org/10.1017/jog.2021.40 Published online by Cambridge University Press

from bulk gas measurements of Antarctic coastal ice core D-10 at a bubble-close-off depth (55 m) by Sowers and others (1989). Furthermore, our findings are consistent with measurements of noble gases, oxygen, and nitrogen in firn air (atmosphere in open pore channels) in the firn–ice transition region, where bubbles are closing off, at polar sites (Huber and others, 2006; Severinghaus and Battle, 2006). After accounting for well-known gravitational effects (Craig and others, 1988), they found systematic enrichments of elemental ratios of Ne/He, O_2/N_2, O_2/Ar and Ar/N_2 with depth. These observations have been interpreted as a result of molecular-size-dependent gas fractionation during bubble formation: small gases, such as Ne, O_2 and Ar are preferentially excluded from shrinking or occluding bubbles (Ikeda and others, 1999; Ikeda-Fukazawa and others, 2001). These gases, therefore, accumulate in the residual firn air. It is noteworthy that the molecular weight of O_2 is greater than that of N_2, although the van der Waals diameter of O_2 is smaller than that of N_2 (Ikeda and others, 1999). Using molecular dynamics simulations, Ikeda-Fukazawa and others (2004) confirmed that the effective molecular size, rather than the molecular mass, is important for gas diffusion through the ice lattice.

The variety of N_2/O_2 values observed at 90 m (Table 1) indicates clearly that the degree of gas fractionation is variable between the air bubbles, even at the same depth. The stochastic nature of bubble formation might be responsible for this phenomenon: the earlier the air bubbles form (the longer duration), the further gas fractionation progresses. As reported by Burr and others (2018), progressive closure of pores takes place in firn. To investigate the gas fractionation after bubble formation in firn, Kobashi and others (2015) analyzed δAr/N_2 data from the GISP2 (Greenland Ice Sheet Project 2), North GRIP (North Greenland Ice Core Project) and Dome Fuji ice cores by using a numerical model of gas loss from air inclusions (Ikeda-Fukazawa and others, 2005). They found that air bubbles formed in the shallow firn are so depleted in δAr/N_2 at the bubble close-off depth and thus dominate the total δAr/N_2 changes in spite of their smaller air contents.

At Vostok, five bubbles were measured at the surface. Six bubbles were analyzed at 83 m (Ikeda and others, 1999). The average composition ratios of N_2 and O_2 for the bubbles were 3.9 at the surface. That for the 83 m was 3.7. The observed range of N_2/O_2 values at the deeper depth (3.2–4.1) was slightly wider than at the surface (3.8–4.1). For these measurements, experimental error (reproducibility of each N_2/O_2 measurement) was not shown. Although their N_2/O_2 values were close to the atmospheric ratio at both depths, it seems that the earlier observations were consistent with the discussion above in terms of an increase in the N_2/O_2 variety with depth.

As described herein, we demonstrate that the application of pure rotational Raman spectroscopy improves the efficiency of the N_2/O_2 analysis of air bubbles in polar firn considerably. For a comprehensive understanding of gas separation processes between the air bubbles and open pores in polar firn, systematic N_2/O_2 measurements for polar firn cores using the new methods presented herein are now underway.

Acknowledgements. We thank all participants for fieldwork, ice sampling, and logistic support. The present research is supported by a Grant-in-Aid for Scientific Research on Creative Scientific Research, Japan. This study was supported by MEXT/JSPS KAKENHI grants 18H05292 and 18H05294, the Joint Research Program of the Institute of Low Temperature Science, Hokkaido University, and the General Collaboration Project of the National Institute of Polar Research.

References

Atkins P and Paula J (2014) *Atkins' Physical Chemistry*, 10th Edn, Oxford: Oxford University Press.

Bender ML (2002) Orbital tuning chronology for the Vostok climate record supported by trapped gas composition. *Earth and Planetary Science Letters* **204**, 275–289. doi: 10.1016/S0012-821X(02)00980-9.

Burr A and 5 others (2018) Pore morphology of polar firn around closure revealed by x-ray tomography. *Cryosphere* **12**, 2481–2500. doi: 10.5194/tc-12-2481-2018.

Craig H, Horibe Y and Sowers T (1988) Gravitational separation of gases and isotopes in polar ice caps. *Science (New York, N.Y.)* **242**, 1675–1678. doi: 10.1126/science.242.4886.1675.

Cuffey KM and Paterson WSB (2010) *Physics of Glaciers*, 4th Edn, Amsterdam, etc.: Academic Press.

Fujita S and 7 others (2016) Densification of layered firn in the ice sheet at Dome Fuji, Antarctica. *Journal of Glaciology* **62**(231), 103–123. doi: 10.1017/jog.2016.16.

Fujita S, Okuyama J, Hori A and Hondoh T (2009) Metamorphism of stratified firn at Dome Fuji, Antarctica: a mechanism for local insolation modulation of gas transport conditions during bubble close off. *Journal of Geophysical Research* **114**(F3), F03023. doi: 10.1029/2008JF001143.

Gauglitz G and Vo-Dinh T (2003) *Handbook of Spectroscopy*. Weinheim: Wiley-VCH Verlag GmbH & Co. KGaA.

Glebov AL and 5 others (2012) Volume Bragg gratings as ultra-narrow and multiband optical filters. *Proceedings of SPIE* **8428**, 84280C. doi: 10.1117/12.923575.

Huber C and 7 others (2006) Evidence for molecular size dependent gas fractionation in firn air derived from noble gases, oxygen, and nitrogen measurements. *Earth and Planetary Science Letters* **243**, 61–73. doi: 10.1016/j.epsl.2005.12.036.

Igarashi M and 5 others (2011) Dating of the Dome Fuji shallow ice core based on a record of volcanic eruptions from AD1260 to AD2001. *Polar Science* **5**(4), 411–420. doi: 10.1016/j.polar.2011.08.001.

Ikeda-Fukazawa T and 5 others (2005) Effects of molecular diffusion on trapped gas composition in polar ice cores. *Earth and Planetary Science Letters* **229**, 183–192. doi: 10.1016/j.epsl.2004.11.011.

Ikeda-Fukazawa T, Hondoh T, Fukumura T, Fukazawa H and Mae S (2001) Variations in N_2/O_2 ratio of occluded air in Dome Fuji Antarctic ice. *Journal of Geophysical Research* **106**(D16), 17799–17810. doi: 10.1029/2000JD000104.

Ikeda-Fukazawa T, Kawamura K and Hondoh T (2004) Mechanism of molecular diffusion in ice crystals. *Molecular Simulation* **30**, 973–979. doi: 10.1080/08927020410001709307.

Ikeda T and 7 others (1999) Extreme fractionation of gases caused by formation of clathrate hydrtates in Vostok Antarctic ice. *Geophysical Research Letters* **26**(1), 91–94. doi: 10.1029/1998GL900220.

Kawamura K and 17 others (2007) Northern Hemisphere forcing of climatic cycles in Antarctica over the past 360,000 years. *Nature* **448**, 912–916. doi: 10.1038/nature06015.

Kobashi T and 9 others (2015) Post-bubble close-off fractionation of gases in polar firn and ice cores: effects of accumulation rate on permeation through overloading pressure. *Atmospheric Chemistry and Physics* **15**, 13895–13914. doi: 10.5194/acp-15-13895-2015.

Lipenkov V, Raynaud D, Loutre M and Duval P (2011) On the potential of coupling air content and O_2/N_2 from trapped air for establishing an ice core chronology tuned on local insolation. *Quaternary Science Reviews* **30**, 3280–3289. doi: 10.1016/j.quascirev.2011.07.013.

Nakahara J, Shigesato Y, Higashi A, Hondoh T and Langway CC (1987) Raman spectra of natural clathrates in deep ice cores. *Philosophical Magazine B* **57**(3), 421–430. doi: 10.1080/13642818808208514.

Penny CM, Peters RLS and Lapp M (1974) Absolute rotational Raman cross sections for N_2, O_2, and CO_2. *Journal of the Optical Society of America* **64**(5), 712–716.

Petit JR and 18 others (1999) Climate and atmospheric history of the past 420,000 years from the Vostok ice core, Antarctica. *Nature* **399**(6735), 429–436. doi: https://doi.org/10.1038/20859.

Sakurai T and 5 others (2010) A technique for measuring microparticles in polar ice using micro Raman spectroscopy. *International Journal of Spectroscopy* **2010**, ID 384956. doi: 10.1155/2010/384956.

Severinghaus JP and Battle MO (2006) Fractionation of gases in polar ice during bubble close-off: new constraints from firn air Ne, Kr and Xe observations. *Earth and Planetary Science Letters* **244**, 474–500. doi: 10.1016/j.epsl.2006.01.032.

Severinghaus JP, Grachev A and Battle M (2001) Thermal fractionation of air in polar firn by seasonal temperature gradients. *Geochemistry, Geophysics, Geosystems* **2**, 1048. doi: 10.1029/2000GC000146.

Shoji H and Langway CC (1982) Air hydrate inclusions in fresh ice core. *Nature* **298**(5874), 548–550. doi: 10.1038/298548a0.

Sowers T, Bender M and Raynaud D (1989) Elemental and isotopic composition of occluded O_2 and N_2 in polar ice. *Journal of Geophysical Research* **94**(D4), 5137–5150. doi: 10.1029/JD094iD04p05137.

Watanabe O and 12 others (1997) Preliminary discussion of physical properties of the Dome Fuji shallow ice core in 1993, Antarctica. *Proceedings of the NIPR Symposium on Polar Meteorology and Glaciology* **11**, 1–8.

Weikusat C, Freitag J and Kipfstuhl S (2012) Raman spectroscopy of gaseous inclusions in EDML ice core: first results – microbubbles. *Journal of Glaciology* **58**(210), 761–766. doi: 10.3189/2012JoG11J222.

https://doi.org/10.1017/jog.2021.40 Published online by Cambridge University Press